Article:
Ali, M, Bonakdar, T, Ghadiri, M et al. (1 more author) (2015) Particle Breakage in a Scirocco Disperser. Powder Technology, 285. pp. 138-145. ISSN 0032-5910

https://doi.org/10.1016/j.powtec.2015.06.048

PARTICLE BREAKAGE IN A SCIROCCO DISPERSER

Muzammil Ali[1], Tina Bonakdar[1], Mojtaba Ghadiri[1,*] and Arjen Tinke[2]

1. Institute of Particle Science and Engineering, University of Leeds, Leeds LS2 9JT, UK
2. Janssen Research & Development, Department of API Small Molecule Development – Chemical Technology and Process Control, Turnhoutseweg 30, B-2340 Beerse, Belgium

[*]Contact Email: M.Ghadiri@leeds.ac.uk

ABSTRACT

Particle breakage during dry dispersion for particle sizing is of concern, yet little work has been carried out on its quantitative analysis. An integrated experimental and CFD modelling work has been carried out to study the breakage of a weak and friable powder in a Scirocco disperser at various nozzle pressures. Spray-dried burkeite powder is used as a model test material. The breakage of particles is analysed using Malvern Mastersizer 2000. The extent of breakage as a function of particle size and impact velocity is obtained by carrying out controlled breakage tests using the single particle impact test device available in our laboratory. The impact velocity of particles in the disperser at various pressures is evaluated by Eulerian-Lagrangian CFD simulation of the air flow in the unit. Particles of different sizes are found to accelerate to different velocities and break to different extents. Particle breakage is noticeable even at the lowest nozzle pressure. A remarkable unification of breakage data may be obtained when the relative change in the surface area for different particle sizes is expressed as a function of the dimensionless breakage propensity group, η, based on the impact velocity in the Scirocco, obtained from the CFD simulation.

KEYWORDS: particle breakage study; CFD modelling; scirocco disperser modelling.

1. INTRODUCTION

A large number of products in various industries are handled and/or produced in particulate form. Particle size analysis forms an integral feature of feed and product characterisation, ensuring consistency in product attributes and process performance. This is done by a wide variety of techniques, giving different measures of particle size. Currently, the most common method of particle sizing is by laser light diffraction. This can be done by either wet or dry dispersion. For the former the particles are suspended in a liquid, taking appropriate measures for full dispersion. For the latter, they are dispersed by an air jet in a Venturi eductor configuration, such as the Scirocco disperser used by Malvern Mastersizer 2000 and the Rodos disperser used by Sympatec Helos. The particles are entrained into an air jet, accelerated and impacted on or slid along the container walls, causing them to disperse to individual entities, ready for sizing by laser diffraction. For fine and cohesive powders the dispersion/collision energy may be inadequate for dispersion and some clusters may survive. A review of the dispersion methods used in the laser diffraction technique is given by Calvert et al. [1]. Recently Calvert et al. [2] investigated the dispersion of cohesive powders and

related the dispersion efficiency to the powder flowability as described by the cohesive powder flow function.

In contrast, for weak and friable powders, the wall collisions may lead to undesirable particle breakage, adversely affecting particle sizing. Figure 1 is a schematic diagram of the Scirocco disperser unit of the Malvern Mastersizer 2000 laser diffraction system. In a Scirocco disperser, a high pressure air is supplied to the air inlet (port 2), which results in a high velocity jet of air at the nozzle tip. The particles are slowly fed to the top inlet of the disperser (port 1) and get rapidly accelerated as they interact with the high velocity air jet stream. The dispersion of particles takes place as they impacts at the elbow. The dispersed particles exit from the outlet (port 3) and are presented to the laser light for laser diffraction measurements.

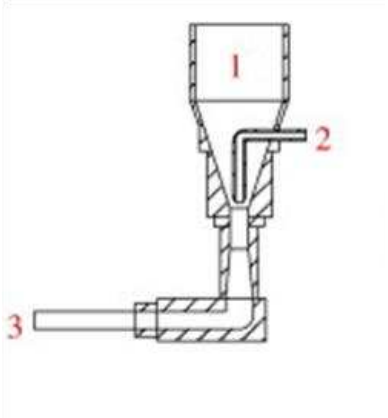

Figure 1. Schematic of Scirocco disperser

Particle strength therefore plays an important role in the reliability of particle size analysis. Extensive studies have been carried out on particle impact by various researchers for the effect of impact energy on the breakage behaviour of particles. Lecoq et al. [3] designed an experimental air-jet mill to study the breakage of particles of a wide range of materials by impacting them on a target at a certain velocity. The experiments were performed in a very dilute regime to minimise particle-particle interactions. The impact behaviour of particles was determined by analysing the size distribution of the impacted particles, obtained by sieving. Dumas et al. [4] studied the impact breakage behaviour of precipitated silica granules by carrying out impact tests. The granules were accelerated using a Venturi system and were impacted against a wall. The particle size distribution (PSD) curves after the impact were determined by laser diffraction in Malvern Mastersizer to give information on the fragmentation mechanisms. Lecoq et al. [5] applied the model by Vogel and Peukert [6] in an air-jet mill to determine the particle grindability parameter. A master-curve was obtained for different materials unifying the data, when the particle grindability parameter was plotted as a function of another parameter characterising the supplied kinetic energy to the materials. Rozinblat et al. [7] carried out experiments in a new horizontal impact breakage device for development and validation of breakage models. The impact velocity of the particles accelerated by the air stream was obtained with a high speed digital camera. Correlations were developed for the breakage probability and breakage kernel as a function of the impact velocity and initial particle size. There is also extensive literature on the breakage and attrition of particles in high-velocity air jets in which particle-particle collisions are the main mechanisms of particle breakage, e.g. Forsythe and Hertwig [8], Gwyn [9], Ghadiri et al. [10], Ghadiri and Boerefijn [11], Boerefijn et al. [12], Bentham et al. [13], Dumas et al. [4], Xiao et al. [14] and Zhang et al. [15].

For the breakage of weak and friable particles there is little quantitative work on the extent of breakage as a function of the nozzle pressure for these dispersers, although there is full awareness and concern about particle breakage during dispersion. Therefore we address this issue here by a combination of experimental impact breakage work on a weak spray-dried powder and modelling of the particle trajectory and hence impact velocity as a function of the nozzle pressure. Three dimensional multiphase Computational Fluid Dynamic simulations of the Scirocco disperser are carried out to analyse the air flow field, following which particle trajectories and impact velocities are calculated using Eulerian-Lagrangian approach. These

calculations are then used in the estimation of the breakage propensity parameter. The extent of breakage and change in the surface area are then related to the breakage propensity parameter.

2. METHODOLOGY

Spray-dried burkeite particles are used as the model test particles as they are highly porous and friable and hence prone to undergo attrition even under gentle handling. Burkeite is a co-crystal of sodium sulphate and sodium carbonate, and it has the general form $Na_4SO_4(CO_3)_t(SO_4)_{1-t}$. The particles of interest in this work have been produced by spray-drying of a slurry of the mixture of two salts [16]. The external shape and internal structure of the particles are shown in the scanning electron micrographs in Figure 2. The breakage of these particles is analysed using the Scirocco dispersion unit and the Malvern Mastersizer 2000 particle size analyser. Different pressures are applied to the nozzle of Scirocco to provide vacuum to entrain the particles into the device. The particles are accelerated by the air flow and impact on an L-bend and are then presented to the laser light for particle size measurement by the laser diffraction method.

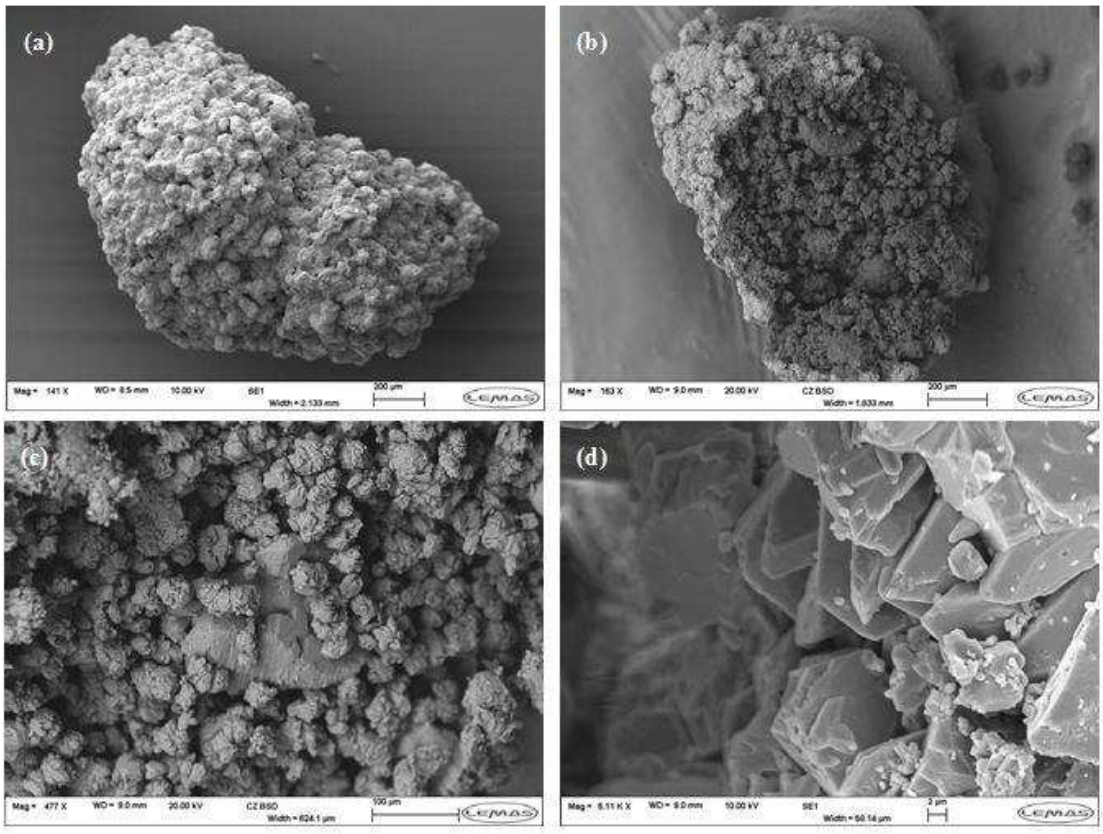

Figure 2. Scanning Electron Microscopy (SEM) images of burkeite showing (a): external shape; (b): internal structure; (c): clusters inside one single particle; (d): crystalline structure of the clusters

The ongoing parallel work indicates structural differences and hence density variations as a function of particle size for spray-dried burkeite. Therefore in order to delineate the effect of particle size and density, it is necessary to use as narrow size distribution as possible and also measure the particle density for each particle size. In order to do this, near-mesh size particles

have been prepared by manually sieving the particles and retrieving only those caught in the mesh opening of the sieve by gentle brushing. The experimental work has been carried out on six near-mesh sizes: 212, 250, 500, 600, 850, 1000 µm. A sufficient quantity of particles is prepared in this way and fed to the Scirocco disperser to get the required obscuration (4 to 8%) for the laser light diffraction. The experiments are carried out at five different nozzle pressures 100, 150, 200, 250 and 300 kPa (corresponding to 1, 1.5, 2, 2.5 and 3 barg) in order to analyse the shift in the particle size distribution as a function of the impact velocity. The particle size distribution is measured by laser diffraction using Mastersizer 2000 and the specific surface areas (SSA) of the dispersed and broken particles are then calculated, based on the particle size distribution and density. In order to calculate the shift in the SSA of the particles as they go through the Scirocco, the SSA of the feed particles needs also to be measured. This is done using Malvern's Spraytec laser diffraction analyser by gently pouring the particles under gravity to its measurement zone. Under such condition little breakage takes place and hence the SSA of the feed can be determined. The characteristics sizes d_{10}, d_{50} and d_{90} of the feed particle size distribution and the associated SSA (calculated) are given in Tables 1 and 2, respectively.

3. EXPERIMENTAL RESULTS AND DISCUSSION

The results of the volume percentage distribution as a function of particle size for the nozzle pressures of 300 kPa are shown in Figure 3 as an example. The characteristic sizes d_{10}, d_{50} and d_{90} of the PSD for the nozzle pressures used in this work are summarised in Table 1. As the nozzle pressure is increased the PSD is shifted to the left indicating particle breakage. At high pressures the particles disintegrate into the constituting crystal aggregates forming the spray-dried particles, hence roughly similar debris sizes are obtained for all particle sizes. At the lowest nozzle pressure the trend is not monotonous as the particles undergo fragmentation, and the fragment size depends on feed particle size, and in turn on the impact velocity, as well as the structure.

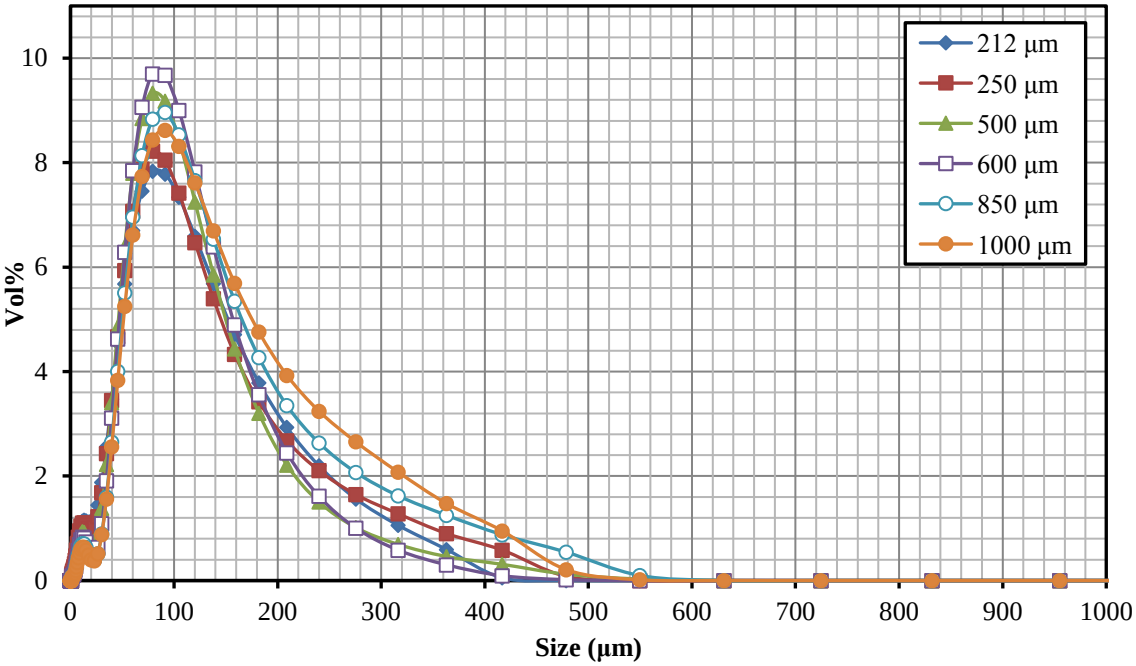

Figure 3. Particle size distribution for different near-mesh particle sizes at 300 kPa nozzle pressure

Table 1. The characteristics sizes d_{10}, d_{50} and d_{90} of the particle size distribution of the feed particles (given by Spraytec) and of the broken particles (given by Mastersizer 2000) in µm for different nozzle pressures given

Size (µm)	212			250			500			600			850			1000		
Pressure (kPa)	**d_{10}**	**d_{50}**	**d_{90}**	**d_{10}**	**d_{50}**	**d_{90}**	**d_{10}**	**d_{50}**	**d_{90}**	**d_{10}**	**d_{50}**	**d_{90}**	**d_{10}**	**d_{50}**	**d_{90}**	**d_{10}**	**d_{50}**	**d_{90}**
Feed	180	228	288	215	282	374	385	530	718	440	584	757	464	628	801	527	1014	1105
100	35	107	308	34	91	239	39	94	235	44	120	284	45	126	353	43	127	355
150	30	94	269	30	91	270	39	88	205	43	93	239	43	105	309	44	110	316
200	21	82	208	22	78	205	34	78	178	37	84	205	40	97	275	39	104	309
250	17	79	203	21	74	179	29	75	158	34	79	178	33	88	236	38	95	275
300	14	71	178	15	71	157	22	71	157	30	75	157	34	82	206	33	87	233

In the Scirocco disperser, particles accelerate to different velocities before impact, depending on particle size and density, and due to the short acceleration length downstream of the nozzle they never reach their ultimate velocity. Therefore the analysis of particle breakage in Scirocco requires information on the impact velocity and the extent of breakage as a function of particle size and impact velocity. This can be obtained using the particle impact test device [17] available in our laboratory. For this purpose impact breakage tests are carried out on the

above near-mesh sizes at velocities of 2, 3, 4, 6, 8, 11, 14 and 18 m/s. The results are expressed in terms of the extent of breakage, R^*, given by:

$$R^* = \frac{m_{de}}{m_m + m_{de}} \times 100\% \quad (1)$$

where m_{de} and m_m are the mass of debris and mother particles, respectively. The extent of breakage is based on the mass fraction of debris passing two standard sieve sizes below the feed lower sieve size. The results are shown in Figure 4, where R^* is plotted as a function of the particle impact velocity. It is observed that at some impact velocities the larger particle sizes break less than smaller particles; however, the breakage trends are too close to each other. It is generally expected that the extent of breakage increases with particle size and velocity. So the anomalous behaviour is attributed to the structural differences as a function of size, giving rise to envelope density variations, as shown by the X-ray microtomography results.

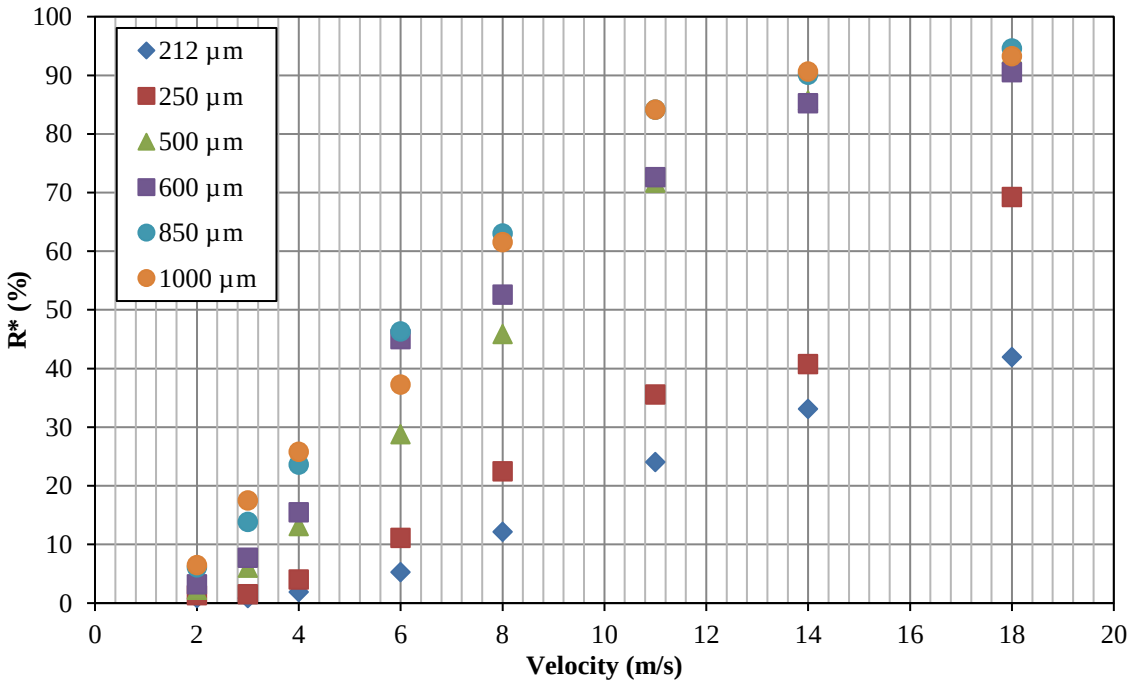

Figure 4. Extent of breakage, R^*, for different near-mesh size particles as a function of impact velocity

For the semi-brittle mode of failure, the extent of breakage is analysed following the model of Ghadiri and Zhang [18], where the extent of breakage follows a square of velocity relationship:

$$R^* = \alpha\eta = \alpha\frac{\rho DH}{K_c^2}V^2 = C\rho DV^2 \quad (2)$$

where D is a linear dimension of the particle, α is the proportionalitty factor, V is the impact velocity and ρ is the envelope density of particles, K_c is the fracture toughness, and H is the hardness of the particles. η is a dimensionless group representing the breakage propensity of materials with a semi-brittle failure mode. The parameter C ($\alpha H/K_c^2$) represents the mechanical properties of the particle that are responsible for plastic deformation and fracture toughness in a lumped parameter format, as otherwise they need to be measured independently, which is difficult for small particles and high strain rates. It should be noted that the same trend in terms of dependence on particle impact velocity and size is expected for

the brittle failure mode based on the work of Vogel and Peukert [6]. So if the extent of breakage is plotted as a function of ρDV^2 a unification of the data is expected for impact velocities in the chipping regime and for different particle sizes with the slope of the line giving the parameter C, provided the variation of density with particle size is taken into account and the mechanical properties are independent of particle size. For this purpose the envelope density of the near-mesh size particles has been measured by X-ray microtomography. Using the estimated density (899, 1077, 1181, 1273, 1382 and 1339 kg/m^3 for particle sizes 212, 250, 500, 600, 850 and 1000 µm), the extent of breakage R^* is plotted as a function of ρDV^2 in Figure 5. It should be noted that large values of R^* correspond to extensive breakage due to fragmentation and they have not been taken into account in the analysis presented in Figure 5, because only the slope of the line in the chipping regime (low values of R^*) represents the lumped parameter C. Clearly a unification of data is achieved for a wide range of particle sizes and impact velocities, and interestingly there is a minimum value of ρDV^2 below which impacts produce little or no chipping. Above this value a linear trend is observed and the best linear regression fit is given in the figure. This information can now be used to interpret the particle breakage in the Scirocco disperser by taking into account the particle impact velocity obtained from the CFD calculations as a function of particle size and density and the lumped parameter C, representing the mechanical properties responsible for breakage.

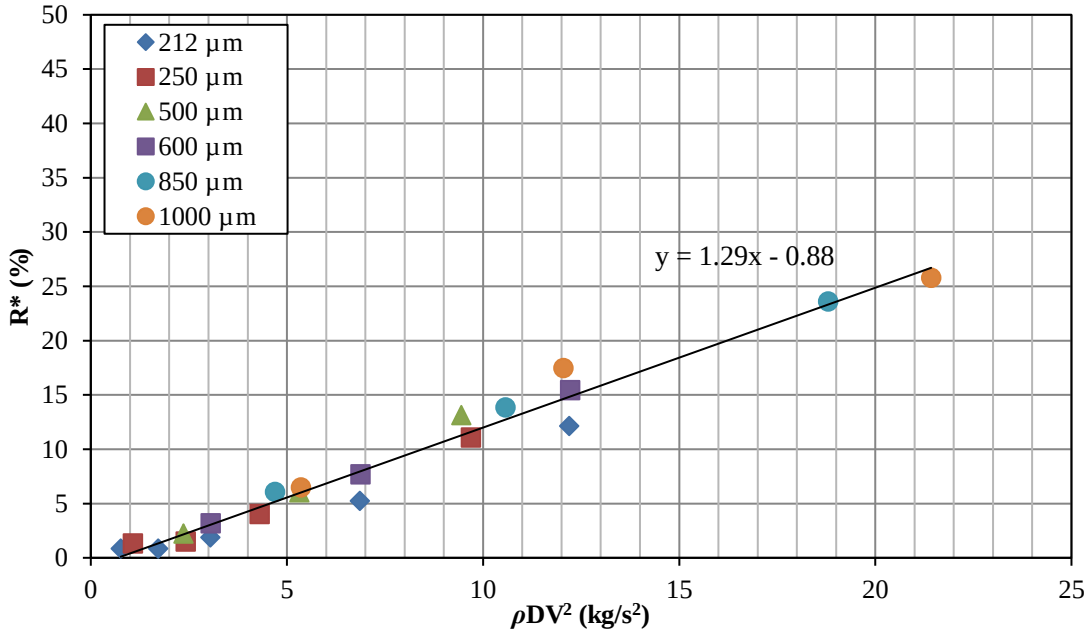

Figure 5. Extent of breakage as a function ρDV^2 with the slope representing $\alpha H/K_c^2$, showing data unification

The specific surface area, SSA, of the feed particles as well as the broken particles are derived from the PSD and envelope density of the particles, given by Mastersizer 2000 as a function of nozzle pressure is given in Table 2. The SSA_0 was measured by Spraytec.

Table 2. The SSA of the feed particles (SSA_0) and broken particles for different near-mesh particle sizes at different nozzle pressures

	SSA (m^2/kg)					
Pressure	**212**	**250**	**500**	**600**	**850**	**1000**

	(kPa)	(µm)	(µm)	(µm)	(µm)	(µm)	(µm)
Spraytec	Feed	29.76	20.19	9.91	8.30	5.27	4.68
Malvern Mastersizer 2000	100	109.22	97.02	75.59	57.99	51.57	53.58
	150	138.31	114.88	85.35	74.08	60.37	61.21
	200	176.23	148.49	112.81	95.68	70.68	66.32
	250	197.31	157.28	128.35	109.55	94.13	83.57
	300	227.63	182.45	143.97	119.93	98.87	92.83

4. CFD MODELLING

4.1 Continuous Phase

The continuous phase is air and its flow is modelled using the time-averaged form of the continuity and Navier-Stokes equations [19]. The turbulence is modelled using the Reynolds stress turbulence model as this model gives a better prediction of fluid velocity profiles in flows involving sudden expansion and in the case of a jet of fluid stream impacting the wall, compared to the eddy viscosity based models. The modelling of flow near the wall is carried out using standard wall functions with smooth wall (zero surface roughness) assumption. The air is considered to be compressible as the density of the air is expected to vary significantly due to large variations in pressure particularly at higher pressures. The steady state assumption is used for the modelling of the continuous phase.

4.2 Discrete Phase

The discrete phase comprises spheres injected from the top of the disperser. The coupling between the air and particles is one-way, i.e. the air flow influences the trajectories of the particles, but the momentum exerted by the particles on the gas phase is ignored. This assumption is valid for particulate flows which are very lean as in the case of Scirocco disperser. The particle trajectory is computed by solving the equation of motion of particles considering the drag, gravitational and buoyancy forces. A widely used spherical drag law proposed by Morsi and Alexander [20] is used for the calculation of drag coefficient. The dispersion of particles due to turbulence is taken into account by enabling the discrete random walk model [21]. The impact of particles on the wall, particularly on the elbow of the disperser, may cause particle breakage, but this is not considered in the model, as the focus is on the incident velocity of the first impact, being the largest velocity of any particles going through the disperser. The restitution coefficient (defined as the ratio between the particle rebound velocity after the wall impact and the incident velocity) is assumed to be 0.5 for all the particle sizes considered.

5. MODEL APPLICATION

5.1 Computational Details, Numerical Solution Method and Initialisation

The meshing of the disperser was carried out using Gambit [22]. The selected mesh comprised 4.1×10^5 primarily tetrahedral cells. The conservation equations for the continuous and discrete phases are solved using the commercial CFD software Fluent v. 12 for compressible flows [21]. For the inlet boundary condition, pressure inlet is specified at the inlet face of the air inlet with values varying for different cases. Pressure outlet with a value

of 0 barg is specified at the outlet face. To enable entrainment of air from the top of the disperser, where the particles are introduced, a pressure boundary condition is specified at the top with a value of 0 barg. For the turbulence boundary conditions, a turbulence intensity of 5% at the corresponding faces along with its diameter is specified.

The pressure-velocity coupling is carried out using PISO scheme [23]; for pressure interpolation, PRESTO! scheme [24] is used. The convective terms are discretised using the second-order upwind discretisation scheme. The convergence criteria for the continuity, momentum and Reynolds stresses were specified as 1×10^{-4}. The simulation was allowed to run until the required level of convergence was met, which was the case for air inlet pressure up to 2.5 barg. At an air inlet pressure of 3 barg the residuals did not reach the required tolerance limit, in this case the simulation was considered to be converged when the level of residuals did not reduce any further after reaching a certain level.

To assess the influence of increasing inlet air pressure on the air velocity profiles and the changes in the predicted particle trajectories, the air pressures considered were 1, 1.5, 2, 2.5 and 3 barg. The simulation cases were named Case 1 to Case 2 for two extreme cases of 100 and 300 kPa. The particle trajectories were calculated in this study. The particle density was varied from 1100 to 1300 kg/m^3, typical of spray-dried burkeite, and the corresponding changes in the impact velocities were quantified. The particle sizes corresponding to sieve sizes 212, 250, 500, 600, 850 and 1000 µm were used, i.e the same as those of the experiments. To obtain statistically representative impact velocity of particles, for each size 200 particles were introduced from a central circular area (10 mm diameter) at the powder inlet face with an initial velocity of 0 m/s into a converged air flow field. The resulting impact velocity of each particle at the elbow was squared and averaged to get the average velocity squared as needed for the calculation of the breakage propensity.

6. MODELLING RESULTS AND DISCUSSION

A plot of contours of the magnitude of air velocity profiles at inlet air pressures of 100 and 300 kPa is given in Figure 6. At all pressures, a jet of air is observed at the nozzle tip. The maximum air velocity is at the neck expansion region. As the jet expands further downstream, the air velocity reduces. The jet does not impinge on to the bend section of the disperser in all the inlet pressures considered. The inlet air pressure significantly influences the maximum velocity of air in the disperser.

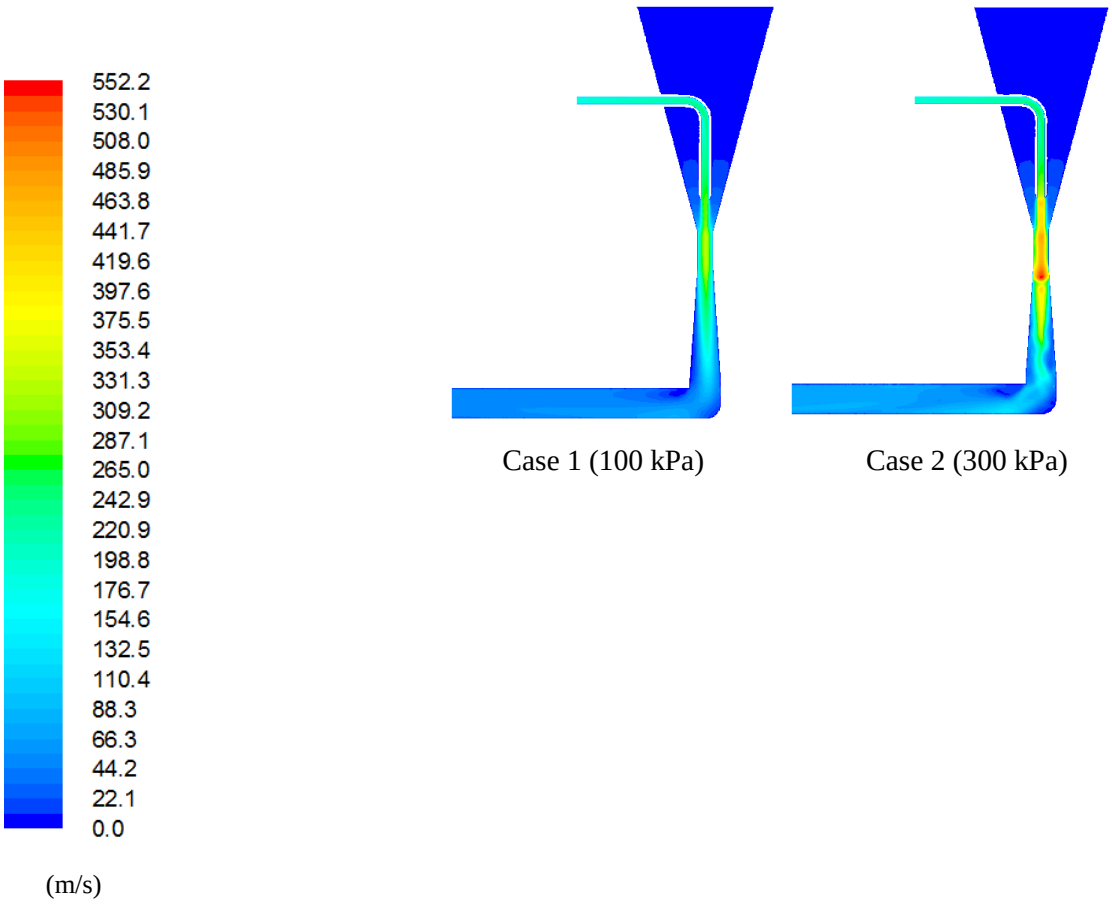

Figure 6. Air velocity profiles inside the Scirocco disperser at 100 and 300 kPa inlet air pressures

The maximum air velocity, V_{air}, at the nozzle tip is 240, 335, 403, 462, 497 and 522 m/s for the nozzle pressures of 100, 150, 200, 250 and 300 kPa, respectively (1, 1.5, 2, 2.5 and 3 barg). At higher pressures, the slope of the line decreases because the air becomes highly compressible and does not obey the linearly increasing relationship.

The particle trajectory calculations were carried out considering particle envelope densities of 1100, 1200 and 1300 kg/m^3. The resulting average impact velocities of particles of different densities were found to increase with decreasing particle densities with a maximum difference of 7% in the predicted impact velocities. The difference in the impact velocity with varying density is not significantly large, hence the results of particles with a density of 1200 kg/m^3 are presented.

Figure 7 is a plot of the average impact velocity as a function of the inlet air pressure. For a given pressure, the smaller particles have a higher impact velocity as compared to the larger particles; this is because the smaller particles have a lower inertia due to smaller mass and get accelerated quicker by the air near the nozzle tip. The highest impact velocity of the smallest particle is at the largest inlet air pressure (about 84 m/s), which is about 6.5 times smaller than the maximum air velocity at the nozzle tip at 300 kPa (3 barg). The average impact velocity of particles increases for all particle sizes with increasing inlet air pressure. The difference in the average impact velocity of the smallest and the largest particle sizes also increases with increasing inlet air pressure. The trend of increasing the impact velocity with increasing

pressure is nearly linear at pressures up to 1.5 barg; however at higher pressures it appears to be reaching a plateau.

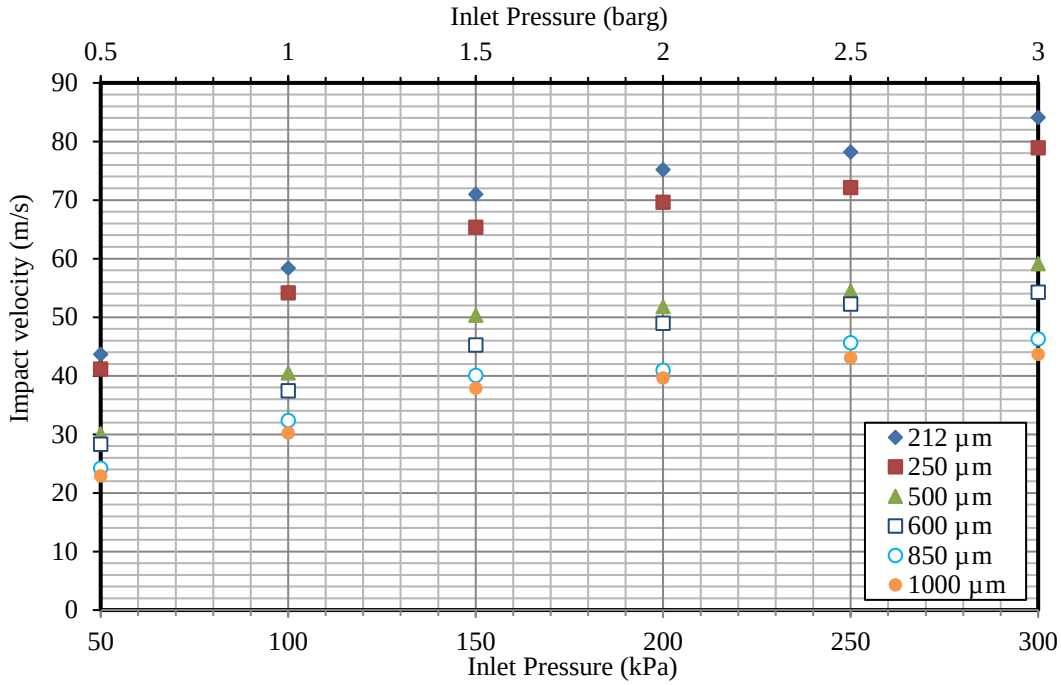

Figure 7. Burkeite particles impact velocities as a function of pressure with a density of 1200 kg/m^3

Figure 8 is a plot of trajectories of particles of two sizes inside the disperser for an inlet air pressure of 100 kPa (1 barg). The trajectories are coloured by the velocity magnitude. The particles fall down initially due to gravity and entrainment of air. They then spread in the top conical region and get accelerated quickly in the neck of the disperser and hit the elbow. After hitting the elbow, the particles bounce back and exhibit multiple collisions with the wall and eventually exit the disperser from the outlet. Smaller particles get more dispersed in the top conical region of the disperser compared to larger particles as the smaller particles have lower inertia. For the same reason, smaller particles have a higher velocity near the nozzle tip and eventually hit the wall with a greater impacting velocity compared to larger particles.

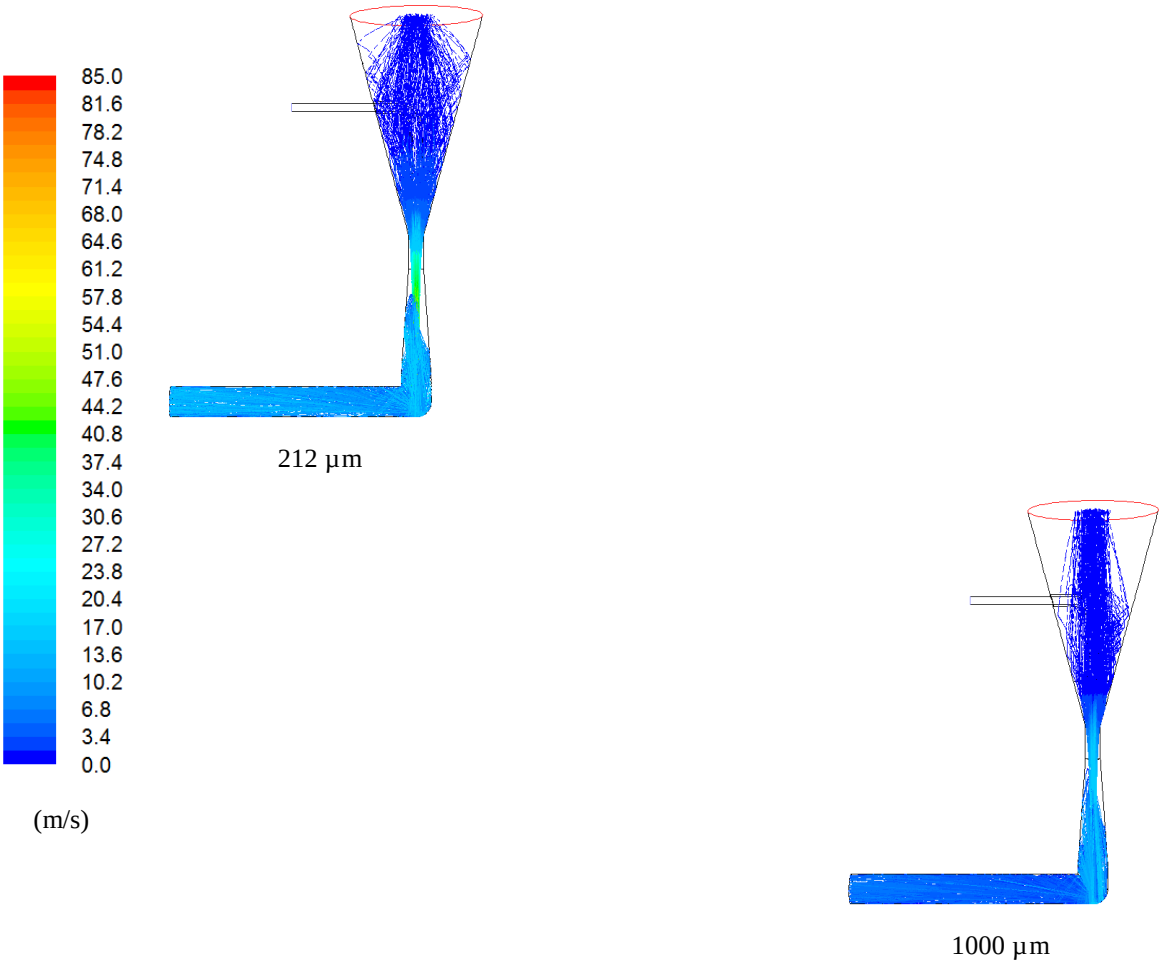

Figure 8. Particle trajectories of burkeite particles of different sizes at 100 kPa (1 barg) inlet pressure.

7. BREAKAGE PROPENSITY OF BURKEITE PARTICLES

The dimensionless group representing the breakage propensity, η, given by equation (2), is calculated using the particle impact velocity obtained from CFD. The SSA_o of the feed particles measured by the Spraytec is given in Table 2 and is used to calculate the relative shift in the SSA, i.e. $\Delta SSA/SSA_o$. The envelope densities of the particles before the test, ρ_m, and after the test, ρ_d, are measured by the above-mentioned method. The average size of the mother particles, d_m, is given by Spraytec, and the average size of debris, d_d, is given by Malvern Mastersizer 2000. The volume-based projected area diameter at random orientation for these nominal sizes, as given by QICPIC (Sympatec, Germany), are 246, 277, 571, 680, 976 and 1197 µm, respectively. This measure of size has been used to calculate η. Equation 2 is based on mass, where the fraction of broken mass (i.e. the extent of breakage as determined by gravimeteric analysis) is related to η [18]. In order to apply this equation to particle breakage in Scirocco, the mass-based extent of breakage has to be converted to surface area ratio. This is given by Equation 3, resulting in additional size and density ratios as shown below:

$$\frac{\rho_d d_d}{\rho_m d_m} \times \frac{\Delta SSA}{SSA_\circ} = \alpha\eta \qquad (3)$$

The results of the surface area ratio, as measured by laser diffraction in Mastersizer 2000, are now plotted as a function of $\alpha\eta(\frac{\rho_m d_m}{\rho_d d_d})$ in Figure 9. A remarkable unification of data is obtained for all particle sizes and impact velocities. It remains to be seen how universal this approach can be by applying it to a wide range of materials. If successful it actually provides a very simple but powerful way to analyse the impact breakage propensity and hence grindability of particulate solids.

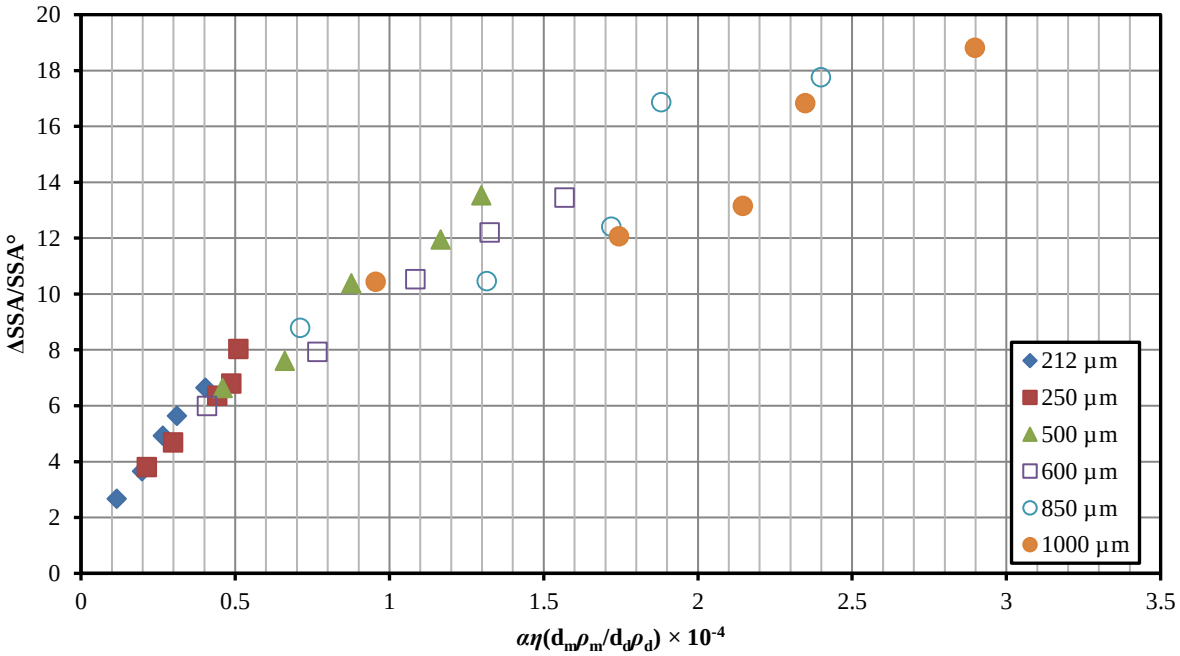

Figure 9. Relative change in the specific surface area as a function of $\alpha\eta(\frac{\rho_m d_m}{\rho_d d_d})$

8. CONCLUSIONS

Particles of different sizes accelerate to different velocities in the Scirocco disperser and break to different extents. For spray-dried burkeite particles, even the lowest nozzle pressure causes notable particle breakage. By characterising their breakage propensity by single particle impact testing and evaluating their impact velocity by CFD, it is found that a remarkable unification of breakage data may be obtained when the relative change in the surface area for different particle sizes is expressed as a function of the dimensionless group representing the breakage propensity, η, based on the impact velocity in the Scirocco, obtained from the CFD simulations.

ACKNOWLEDGEMENT

The authors are thankful to Dr Umair Zafar and Mr Siwarote Siriluck for their help in the operation of laser diffraction instruments.

REFERENCES

[1] Calvert, G., Ghadiri, M. and Tweedie, R. (2009). Aerodynamic dispersion of cohesive powders: A review of understanding and technology. Advanced Powder Technology, vol. 20, pp. 4-16.

[2] Calvert, G., Ghadiri, M., Dyson, M., Kippax, P. and McNeil-Watson, F. (2013). The flowability and aerodynamic dispersion of cohesive powders, Powder Technology, vol. 240, pp. 88-94.

[3] Lecoq, O., Chouteau, N., Mebtoul, M., Large, J. F. and Guigon, P. (2003). Fragmentation by high velocity impact on a target: a material grindability test. Powder Technology, vol. 133, pp. 113-124.

[4] Dumas, T., Bonnefoy, O., Grosseau, P., Thomas, G., Nebut, S. and Guy, L. (2011). New methods to analyse fragmentation mechanisms of precipitated silicas. 5th International Workshop on Granulation, Granulation Conference Lausanne, Switzerland.

[5] Lecoq, O., Chamayou, A., Dodds, J. A. and Guigon, P. (2011). Application of a simplifying model to the breakage of different materials in a air jet mill. Int. J. Miner. Process., vol. 99, pp. 11-16.

[6] Vogel, L. and Peukert, W. (2003). Breakage behaviour of different materials – construction of a mastercurve for the breakage probability. Powder Technology, vol. 129, pp. 101-110.

[7] Rozinblat, Y., Grant, E., Levy, A., Kalman, H. and Tomas, J. (2012). Selection and breakage functions of particles under impact loads. Chemical Engineering Science, vol. 71, pp. 56-66.

[8] Forsythe, W. L. and Hertwig, W. R. (1949). Attrition characteristics of fluid cracking catalysts. Ind. Eng. Chem., vol. 41, pp. 1200-1206.

[9] Gwyn, J. E. (1969). On the particle size distribution function and the attrition of cracking catalysts. AIChE J., vol. 15, pp. 35-39.

[10] Ghadiri, M., Cleaver, J.A.S., Tuponogov, V.G. and Werther, J. (1994). Attrition of FCC Powder in the Jetting Region of a Fluidised Bed. Powder Technology, vol. 80, pp. 175-178.

[11] Ghadiri, M. and Boerefijn, R. (1996). A Model of Attrition in the Jetting Region of Fluidised Beds. KONA Powder and Particle, No. 14, pp. 5-15.

[12] Boerefijn, R., Gudde, N.J. and Ghadiri, M. (2000). A review of attrition of fluid cracking catalyst particles. Advanced Powder Technology, vol. 11, pp. 145-174.

[13] Bentham, A.C., Kwan, C.C., Ghadiri, M. and Boerefijn, R. (2004). Fluidised bed jet milling of pharmaceutical powders. Powder Technology, vol. 141, pp. 233-238

[14] Xiao, G., Grace, J. R. and Lim, C. J. (2012). Limestone particle attrition in high-velocity air jets. Ind. Eng. Chem. Res., vol. 51, pp. 556-560.

[15] Zhang, Q., Jamaleddine, T. J., Briens, C., Berruti, F. and McMillan, J. (2012). Jet attrition in a fluidized bed. Part I: Effect of nozzle operating conditions. Powder Technology, vol. 229, pp. 162-169.

[16] Xu, D. and Martin de Juan, L. (2014). Personal communication.

[17] Ghadiri, M. and Yuregir, K. R. (1987). Impact attrition of NaCl particles. In Tribology in Particulate Technology (ed Briscoe and M. Adams). Cristol, Adam Hilger.

[18] Ghadiri, M., and Zhang, Z. (2002). Impact attrition of particulate solids. Part 1: A theoretical model of chipping. Chemical Engineering Science, vol. 57, pp. 3659-3669.

[19] Versteeg, H. K. and Malalasekera, W. (1995). An Introduction to Computational Fluid Dynamics. Longman Scientific and Technical, Harlow.

[20] Morsi, S. A. and Alexander, A. J. (1972). An investigation of particle trajectories in two-phase flow systems. J. Fluid Mech., vol. 55 (2), pp. 193-208.

[21] Fluent User's guide. (2009). Ansys Inc.

[22] Gambit, (2006). version 2.4, http://www.ansys.com

[23] Issa, R. I. (1985). Solution of the implicitly discretised fluid flow equations by operator splitting. J. Comp. Phy., vol. 62, pp. 40-65.

[24] Patankar, S.V., (1980). Numerical heat transfer and fluid flow. Hemisphere, Washington.